

Journal of Mechanics of Materials and Structures

AUTOMATIC GENERATION OF STATICALLY ADMISSIBLE STRESS FIELDS IN MASONRY VAULTS

Elena De Chiara, Claudia Cennamo, Antonio Gesualdo, Andrea Montanino, Carlo Olivieri
and Antonio Fortunato

Volume 14, No. 5

December 2019



AUTOMATIC GENERATION OF STATICALLY ADMISSIBLE STRESS FIELDS IN MASONRY VAULTS

ELENA DE CHIARA, CLAUDIA CENNAMO, ANTONIO GESUALDO,
ANDREA MONTANINO, CARLO OLIVIERI AND ANTONIO FORTUNATO

The objective of the present work is to develop an automated numerical method for the analysis of thin masonry shells. The material model for masonry that we adopt is the so-called “normal rigid no-tension” (NRNT) material; and for such a material, the kinematical and the safe theorems of limit analysis are valid. The present study focuses on the application of the second theorem to masonry vaults and domes, being devoted to the determination of a class of purely compressive stress regimes, which are balanced with the load. The mere existence of such a class is a proof that the structure is safe, and members of this class may be used to assess the geometric degree of safety of the structure and to estimate bounds on the thrust forces exerted by the structure on its boundary. The problem is reduced to the equilibrium of a membrane S and can be formulated in terms of projected stresses defined on the planform Ω of S . The search of the stress reduces to the solution of a second-order pde, in terms of the stress potential F . In order that the membrane stress on S be compressive, the potential F must be concave. As for the thrust line in an arch, the surface S is not fixed and may be changed, given that it remains inside the masonry. Under these simplifying assumptions, the whole class of equilibrated stress regimes for a masonry shell is obtained by moving and deforming S inside the masonry, and also, for any fixed shape, by changing the boundary data for F , that is the distribution of thrust forces along the boundary. The search for a feasible stress state on a convenient membrane surface, to be chosen with a trial and error procedure, requires a substantial effort and may be unrewarded. Then, the main object of the present work, is to produce a computer code that can handle numerically the interplay of the shape controlled by a function f , and of the stress potential F , by developing a convergent optimization scheme able to give a safe state under the given material and geometrical constraints, namely the concavity of F and the inclusion of f within the masonry. Two simple cases, are exposed in detail to illustrate the method.

1. Introduction

A particularly simple and efficient way to approach the structural analysis of masonry is to adopt for the material the model of Heyman [1966]. This model is based on three strong simplifying assumptions: the material is unilateral (no-tension), it cannot slide, and is infinitely rigid and resistant in compression. In this context there are a number of themes that are still at cutting edge of research, namely: doing unilateral with a computer (see [Angelillo et al. 2010; Bruggi and Taliercio 2015]), studying the effects of settlements [Cennamo et al. 2017], predicting fracture patterns produced by settlements in masonry structures and, vice versa, identifying the causes of a given fracture pattern (see [Iannuzzo et al. 2018]), assessing the equilibrium of masonry vaults under vertical and horizontal forces [Angelillo and Fortunato 2004;

Keywords: masonry vaults, no-tension materials, Airy’s stress function, Pucher equilibrium.

Block et al. 2006], studying dynamical effects as in [DeJong and Dimitrakopoulos 2014] or in [Monaco et al. 2014; Gesualdo et al. 2014; 2018a; 2018b]. The formulation of the boundary value problem for unilateral masonry materials (that is, the NRNT materials for which the latent strains, known as fractures, satisfy a normality condition with respect to the admissible stresses) can be found in [Angelillo 2014]. For such a material, the kinematical and the safe theorems of limit analysis are valid and can be applied to different structures as can be seen in [Heyman 1966; Koocharian 1952; Livesley 1978] as well as in [Como 1992; Angelillo 2014; 2015; Brandonisio et al. 2015; Gesualdo et al. 2017; Angelillo et al. 2014; 2016; Fortunato et al. 2014; 2016; 2018; Iannuzzo et al. 2018].

Indeed, the more efficient tool that can be introduced for applying the unilateral no-tension model to masonry structures is the systematic use of singular stress and strain fields, within the framework defined by the two theorems of limit analysis (see [Angelillo et al. 2014], for applications of the safe theorem and [Fortunato et al. 2014], for applications of the kinematic theorem to walls).

The objective of the present work is to develop an automated numerical method for the analysis of thin masonry shells made of NRNT materials.

The more recent literature on masonry-like vaults is rather vast; apart from the production of the school of Salerno, originated by the paper on the lumped stress method [Fraternali et al. 2002a], and applied to vaults in [Fraternali et al. 2002b; Block et al. 2006; Fraternali 2010], and recently in [Angelillo et al. 2013; Marmo and Rosati 2017; Marmo et al. 2018], we recall the pioneering work by O'Dwyer [1999], and the works in [Block 2009; Block et al. 2006; Vouga et al. 2012; De Goes et al. 2013; Block and Lachauer 2014; Miki et al. 2015]. The case of spiral stairs, treated with a classical elastic membrane model by Calladine [2005], was also considered with the unilateral model in [Block 2009; Angelillo 2015; 2016; De Serio et al. 2018; Gesualdo et al. 2017].

In the spirit of the safe theorem, the vault structure is stable if a statically admissible stress field can be constructed. On allowing for singular stresses, here we consider statically admissible stress fields concentrated on surfaces or lines lying inside the masonry vault. Such structures are unilateral membranes/arches, whose geometry is described as Monge, and the equilibrium of them is formulated in Pucher form, that is, in terms of the so-called projected stresses over the planform Ω .

In particular, the method we propose is devoted to the determination of a class of purely compressive stress regimes, which are balanced with the load. The mere existence of such a class is a proof that the structure is safe, and members of this class may be used to assess the geometric degree of safety of the structure and to estimate bounds on the thrust forces exerted by the structure on its boundary.

The main simplifications we make to conduct our analysis concern the load and the type of internal stress that we consider: (i) the main part of the internal stress is a membrane stress concentrated on a surface S located inside the masonry, and (ii) the external load is lumped in such a way that it can be transferred to the surface S as a distributed load per unit area.

Under these simplifying assumptions, the equilibrium problem for the membrane S can be formulated in Pucher form (see [Angelillo and Fortunato 2004; Angelillo et al. 2013; Pucher 1934; Heyman 2012]), in terms of projected stresses defined on the planform Ω of S . The search for the stress reduces to the solution of a second-order pde, in terms of the stress potential F . In order that the membrane stress on S be compressive, the potential F must be concave [Angelillo et al. 2010; Fraternali et al. 2002a].

As for the thrust line in an arch, the surface S is not fixed and may be changed, given that it remains inside the masonry. Under these simplifying assumptions, the whole class of equilibrated stress regimes

for a masonry shell, is obtained by moving and deforming S inside the masonry, and also, for any fixed shape, by changing the boundary data for F , that is, the distribution of thrust forces along the boundary.

A masonry shell is a 3D structure which is somehow thin, the usual slenderness (span/thickness ratio) ranging between 20 and 50. Despite this relative slenderness, given that the shape enters the second-order pde with its Hessian, even small changes of the shape of S in a neighbourhood of the middle surface, may alter sensibly the solution in terms of F , that is, of the resulting stresses.

2. Outline of the method

The unilateral restrictions require that the membrane surface lies in between the extrados and intrados surfaces of the vault and that the stress function be concave. Such last constraint is, in general, not satisfied on a given shape for given loads: in such a case, the shape has to be modified to fit the constraint. In a sense, the unilateral assumption renders the membrane an underdetermined structure that must adapt its shape in order to satisfy the unilateral restrictions. The search for a feasible stress state on a convenient membrane surface has been conducted so far iteratively by trial and error; this sort of manual procedure, based on a skillful ansatz either on the initial shape (that is, on the function f describing S) or on the initial projected stress (that is, on F), requires a substantial effort and may be unrewarded. Therefore, the main object of the present work is to produce a computer code that can handle numerically the interplay of the shape f and the stress potential F by developing a convergent optimization scheme capable of producing a safe state under the given material and geometrical constraints, namely the concavity of F and the inclusion of f within the masonry.

The way we propose here for constructing a convergent iterative scheme, stems from the variational approximation of the transverse equilibrium equation, obtained by discretizing both the shape f and the stress potential F on the same grid. On adopting a simplicial representation of both surfaces, the curvature of these surfaces is singular, and an efficient method of approximating the Hessian is required; we adopt a lumped stress method (LSM) type approximation (see [Fraternali et al. 2002a]). One may start the iterative procedure by giving either an initial tentative simplicial shape f^0 or a tentative simplicial stress potential F^0 . If f^0 is assigned and the boundary values F^* of F are prescribed, the solution of the approximate variational equation will give a corresponding potential $F(f^0, F^*)$, balanced with the transverse loads. Since the problem at hand is linear, it can be formalized as

$$A(f^0)F = b(F^*), \quad (1)$$

$A(f^0)$ being a linear operator. By solving for F one obtains

$$F(f^0, F^*) = A^{-1}(f^0) b(F^*). \quad (2)$$

An objective function $\text{Conc}(F)$, measuring the degree of concavity of the stress potential $F(f^0, F^*)$ over the domain, can be introduced. By assuming that the shape f^0 is fixed and the boundary data F^* are unknown, if one makes explicit $\text{Conc}(F)$ in terms of F^* , say $C(F^*) = \text{Conc}(A^{-1}(f^0) b(F^*))$, the optimum problem for the objective function $C(F^*)$, can be formulated, and the best choice for the datum F^* for the given discretization and the given shape f^0 can be determined. If the resulting solution F_{opt} is concave, the iterative procedure stops, otherwise, the stress potential F_{opt} is concavified into a new concave stress potential F^0 with a convex hull type technique; the resulting stress potential F^0 is

used as the starting point for a second step in which the roles of f and F are interchanged. In this second step, the objective function to be optimized in terms of the boundary state f^* is changed into a norm of the distance of the form f from the mean surface.

3. Equilibrium formulation

3.1. Geometry. The geometry of a vault can be described by its intrados and extrados surfaces and by the geometry of the filling. With our model, it is assumed that the load applied to the vault is carried by a membrane structure S of thickness s . The geometry of the membrane S is not fixed, in the sense that it can be displaced and distorted, provided that it lays inside the masonry. The surface S that we consider, is continuous but not necessarily smooth, and to describe it we can adopt Monge representation.

The unit vectors associated to the fixed Cartesian reference system are denoted as $\{\hat{e}_1, \hat{e}_2, \hat{e}_3\}$. The position vector \mathbf{x} of a point of the surface is given by

$$\mathbf{x} = x_1 \hat{e}_1 + x_2 \hat{e}_2 + f(x_1, x_2) \hat{e}_3, \quad \{x_1, x_2\} \in \Omega, \quad (3)$$

where Ω is a plane two-dimensional connected domain, called the planform of S , whose boundary $\partial\Omega$ is composed of a finite number of closed curves, of outer normal \mathbf{n} ; $\{x_1, x_2\}$ are the Cartesian coordinates of S in the planform Ω , and the curvilinear coordinates on S ; $x_3 = f(x_1, x_2)$ is the rise of the membrane with $f \in C^0(\Omega)$.

A three-dimensional view of S is shown in Figure 1 (left). A couple of coordinate lines x_1 and x_2 are depicted in Figure 1, along with a magnified view of a differential element of the shell bounded by arcs of coordinate lines (Figure 1, right). The membrane is loaded by the external forces \mathbf{q} per unit area of S and held in equilibrium by the membrane stresses \mathbf{T} (for the components of \mathbf{T} see Figure 1, right). The natural or covariant base vectors \mathbf{a}_i tangent to S are represented in Figure 1 (middle). With \mathbf{a}_i we denote the dual bases.

3.2. Membrane equilibrium in Pucher form. Here we follow essentially the developments contained in [Fortunato et al. 2014], repeating the essential ingredients of the analysis only for completeness. The generalized membrane stress on S is defined by the surface stress tensor \mathbf{T} , represented in the covariant base as

$$\mathbf{T} = T^{\alpha\beta} \mathbf{a}_\alpha \otimes \mathbf{a}_\beta. \quad (4)$$

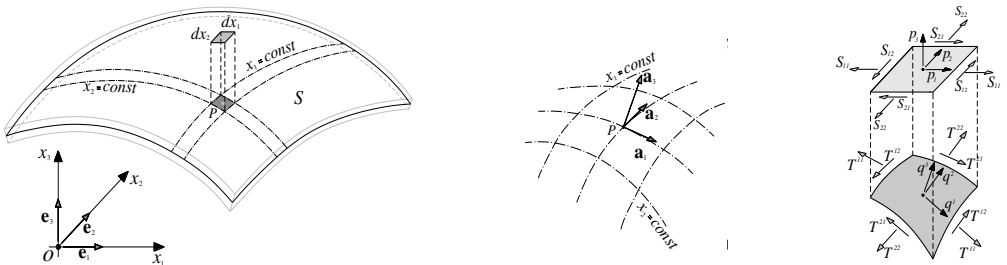


Figure 1. Membrane and surface stresses (left), covariant basis (middle), shell element and stresses (right).

In (4), $T^{\alpha\beta}$ are the contravariant components of \mathbf{T} and the summation convention over repeated Greek indices: $\alpha, \beta, \gamma, \dots = 1, 2$, has been adopted. Contravariant components of stress are convenient but are nonphysical, and we will need to transform them into Cartesian ones in order to read more easily the results of the analysis.

In the equilibrium equations, the divergence of the generalized surface stress \mathbf{T} balances the load $\mathbf{q} = \{q_1, q_2, q_3\}$, defined per unit surface area on S :

$$\frac{\partial}{\partial x_\gamma} (T^{\alpha\beta} a_\alpha \otimes a_\beta) a^\gamma + \mathbf{q} = \mathbf{0}. \quad (5)$$

The most efficient way to describe membrane equilibrium of a thin shell under a load \mathbf{q} is due essentially to Pucher [1934]. The generalized contravariant stress components $T^{\alpha\beta}$ on the membrane surface are transformed into projected stress components $S_{\alpha\beta} = J T^{\alpha\beta}$ in the planform, being $J = \sqrt{1 + f_{,1}^2 + f_{,2}^2}$ the *Jacobian* determinant, that is, the ratio between the differential surface area on S and its projection on the planform Ω . Denoting $\mathbf{p} = J\mathbf{q}$ the load per unit projected area. In the case of pure vertical loading $\mathbf{p} = \{0, 0, -p\}$, and the problem may be solved by introducing the *Airy stress function* $F(x_1, x_2)$ (here we assume only continuous surfaces) in the form

$$S_{11} = F_{,22}, \quad S_{22} = F_{,11}, \quad S_{12} = S_{21} = -F_{,12}. \quad (6)$$

The first two equilibrium equations are identically solved by (6), and we are left with a single equation in the transverse direction as reported with more details in [Gesualdo et al. 2014; Angelillo et al. 2013].

The transverse equilibrium equation corresponds to the balance of the vertical component of the force $p_3 = -p$ with the scalar product of the Pucher stress matrix times the Hessian of the function f in its covariant form. In terms of the Airy's stress function, it can be written as

$$F_{,22} f_{,11} + F_{,11} f_{,22} - 2F_{,12} f_{,12} = p. \quad (7)$$

3.3. Singular stress and the equilibrium of unilateral membranes. We describe the masonry as a continuum made of NRNT materials in the sense of Heyman, therefore the following material restrictions are imposed: the generalized stress \mathbf{T} is a negative semidefinite and does no work for the corresponding strain \mathbf{E} , that is, a positive semidefinite:

$$\mathbf{T} \in \text{Sym}^-, \quad \mathbf{E} \in \text{Sym}^+, \quad \mathbf{T} \cdot \mathbf{E} = 0. \quad (8)$$

The first application of Pucher's transformation for NT masonry vaults can be found in [Angelillo and Fortunato 2004], where it is shown that, due to the NT constraint, both the surface stress tensor and the matrix of the projected stresses must be negative semidefinite. In terms of the stress function F , this condition can be written as

$$F_{,11} + F_{,22} \leq 0, \quad F_{,11} F_{,22} - F_{,12}^2 \geq 0, \quad (9)$$

hence $F(x_1, x_2)$ is concave.

If F is only continuous, it may exhibit folds; if so, the projected stress is a line Dirac delta with support along the projection Γ of the fold on Ω . The *Hessian* \mathbf{H} of F is singular transversely to Γ , namely a uniaxial singular part parallel to the unit vector \mathbf{h} normal to Γ . Correspondingly the directional derivative

of F in the direction of \mathbf{h} , denoted F_h , presents a jump. Therefore, the singular part of the Hessian \mathbf{H} of F can be written as

$$\mathbf{H}_s = \delta(\Gamma) \Delta F_h \mathbf{h} \otimes \mathbf{h}, \quad (10)$$

$\delta(\Gamma)$ being the unit line Dirac delta on Γ and ΔF_h the jump of slope along the direction \mathbf{h} . Due to the relation (6), the singular part of the projected stress, corresponding to F , is a line Dirac delta on Γ of the form

$$\mathbf{S}_s = \delta(\Gamma) \Delta F_h \mathbf{k} \otimes \mathbf{k}, \quad (11)$$

where \mathbf{k} is the unit vector tangent to Γ . The concavity of F implies the concavity of the fold Γ . Then ΔF_h is negative and the corresponding projected singular stress concentrated on Γ is compressive.

As a consequence of the previous analysis, the equilibrium problem for the unilateral membrane S , under pure vertical loading, consists in finding a concave stress function $F(x_1, x_2)$ satisfying equation (7), with boundary conditions of Dirichlet or Neumann type, namely

$$F(x_1(s), x_2(s)) = g(s), \quad \text{or} \quad \frac{dF}{dn}(x_1(s), x_2(s)) = h(s), \quad \text{on } \partial\Omega, \quad (12)$$

s being the parametrization of the boundary $\partial\Omega$ with the arc length, and $g(s)$, $h(s)$ the contact internal moment and axial force produced by the allied tractions, on a 1D beam structure having the shape of the curve $\partial\Omega$. We also notice that the normal and shear components σ , τ of the tractions applied along the boundary, can be defined in terms of the boundary data g , h , as

$$\sigma(s) = g_{/ss}(s), \quad \tau(s) = h_{/n}(s), \quad (13)$$

where $/$ denotes the covariant derivative with respect to s , n along the boundary.

4. Computational scheme

4.1. Simplicial approximation of f^0 . To illustrate the procedure, we consider two examples: a cloister vault and a domical vault, both based on a rectangular planform Ω . As initial shape function f^0 , an approximation of the middle surface of the vault, obtained by discretizing the Monge description of this surface over a triangular grid (described below), is considered (Figure 2).

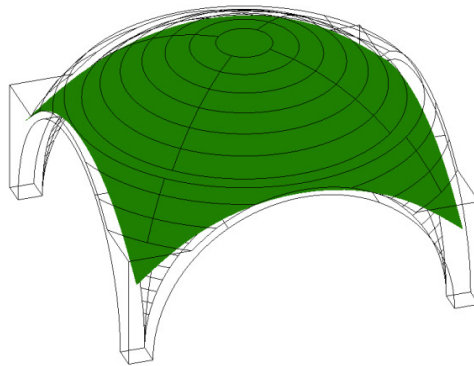


Figure 2. Initial choice for the shape function.

4.2. Variational formulation of the equilibrium. For approximating the solution of the equilibrium problem, we refer to the variational formulation of equation (7). As can be seen in [Giaquinta and Giusti 1985] and more specifically for vaults in [Angelillo and Fortunato 2004] and [Fraternali 2010], we impose the stationarity of the functional:

$$E(F) = \frac{1}{2} \int_{\Omega} a_{\alpha\beta} F_{,\alpha} F_{,\beta} da + \int_{\Omega} p F da, \quad (14)$$

where the matrix $\{a_{\alpha\beta}\}$ is the $\pi/2$ rotation of the Hessian \mathbf{H} of f^0 .

Indeed, it is easy to show that equation (8)₃ can be obtained as the Euler equation associated to the condition

$$\delta E(F) = 0, \quad (15)$$

if Dirichlet type boundary conditions are considered.

4.3. Definition of the meshes. The region Ω is discretized considering two complementary and overlapping meshes, the primal mesh: $\Pi_M = \{\Omega_i, i \in 1, \dots, M\}$, M being the number of triangular elements of the mesh (Figure 3, left), and the dual mesh: $\Pi_N = \{\Omega_i, i \in 1, \dots, N\}$, N being the number of elements of the dual mesh, that is, the number of nodes of the primal mesh (Figure 3, right). In our examples, the primal mesh is a regular triangular mesh, the dual mesh is formed by equal hexagons whose centroids are the nodes of the primal mesh. The skeleton of the primal mesh is used to approximate the stress field through uniaxial singular stresses while the dual mesh is used to average such singularities in the neighborhood of each primal node with an LSM-type approximation (see [Fraternali et al. 2002a]). In this way the final description of the stress field is a piecewise constant field over the dual mesh.

In order to allow the calculation of both the Hessian \mathbf{H} of f and F on the boundary of the vault, we enlarge the domain for the two meshes with respect to the actual planform. To this end, a one element strip of fictitious elements is added all around the original domain. Therefore, we have an additional mesh: $\Pi'_{M'} = \{\Omega_i, i \in 1, \dots, M'\}$, M' being the number of triangular elements of the fictitious part of the mesh.

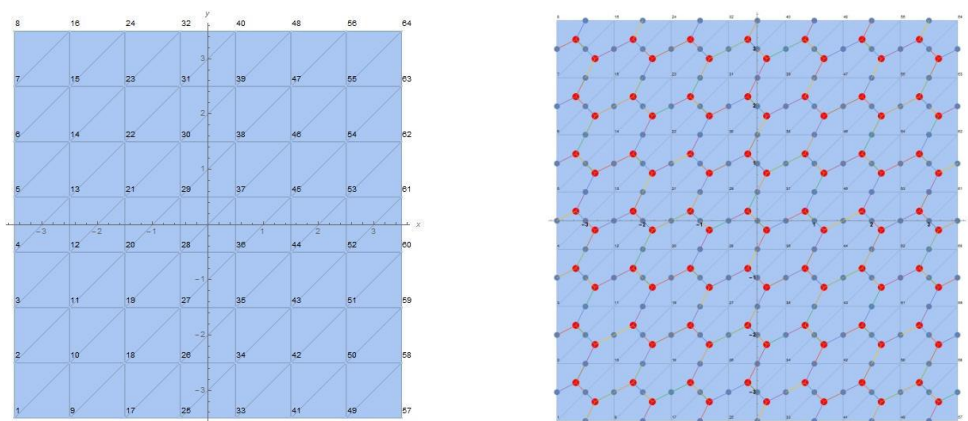


Figure 3. Primal mesh (left) and dual mesh (right) for the mesh 1.

4.4. Approximation of the curvature of f^0 . Once the initial shape f^0 is chosen and approximated over the given triangular grid, we use the same mesh to discretize problem (15). The surface S^0 (and any other surface S obtained during the iteration process) is piecewise linear, the simplicial surface being generated by the list as the values that f^0 takes at the nodes of the primal mesh:

$$\hat{S}^0 = \{x_1(i), x_2(i), f^0(i)\}, \quad i \in \{1, 2, \dots, N\}. \quad (16)$$

We also introduce the list of nodal values:

$$\hat{f}^0 = \begin{Bmatrix} f^0(1) \\ f^0(2) \\ \dots \\ f^0(N) \end{Bmatrix}. \quad (17)$$

The Hessian of f^0 is singular, being represented by line Dirac deltas $\delta(\Gamma)$, applied along the skeleton of the mesh. Such singular field is transformed into a piecewise constant field over the dual mesh through a LSM type approximation scheme as

$$H(\hat{f}^0)_j = \frac{\sum_i \Delta f^0(i) l(i) \hat{\mathbf{h}}(i) \otimes \hat{\mathbf{h}}(i)}{\text{area}(\hat{\Omega}_j)}, \quad j \in \{1, 2, \dots, N\}, \quad i \in \{1, 2, \dots, m_j\}, \quad (18)$$

$\Delta f^0(i)$ being the jump of the gradient of f across the edge i , in the direction orthogonal to the edge, and $l(i)$ the length of the edge i , $\hat{\mathbf{h}}(i)$ the unit normal vector of the edge i , m_j the number of the edges of the dual element at the generic node j (in our case, $m_j = 6$ for the inner nodes).

To reduce the apparent anisotropy effect introduced by the mesh, especially for rough discretizations, we consider two different primal meshes (mesh 1, mesh 2) characterized by opposite diagonals. The final solution, reached at the end of each step of the iteration, will then be averaged by combining linearly the results obtained by employing mesh 1 and mesh 2. To completely formulate the discretized problem, we have to impose the boundary conditions for the stress function F .

4.5. Variational approximation of ∇F . The gradient list associated to the primary mesh is defined by

$$\nabla F = \begin{Bmatrix} \begin{bmatrix} F_{,1} \\ F_{,2} \end{bmatrix}_1 \\ \begin{bmatrix} F_{,1} \\ F_{,2} \end{bmatrix}_2 \\ \dots \\ \begin{bmatrix} F_{,1} \\ F_{,2} \end{bmatrix}_M \end{Bmatrix}, \quad (19)$$

denoting 1, 2, 3 the nodes of a generic primal element, for each triangle the gradient is calculated as

$$\text{fun } F = F(1) + \alpha(F(2) - F(1)) + \beta(F(3) - F(1)), \quad \nabla F = \frac{\partial \text{fun } F}{\partial \alpha} \mathbf{b}^1 + \frac{\partial \text{fun } F}{\partial \beta} \mathbf{b}^2, \quad (20)$$

where $\mathbf{b}^1, \mathbf{b}^2$ are the base vector dual to the vectors $\mathbf{b}_1, \mathbf{b}_2$ shown in Figure 4 and $F(i)$ the values that the stress function assumes at the nodes of the considered triangle (see Figure 4).

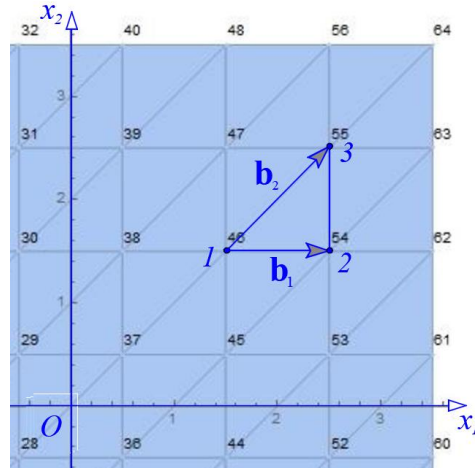


Figure 4. Natural element base.

4.6. Dirichlet data. We choose Dirichlet type boundary conditions considering the value of F at the boundary. In particular, we approximate σ (see (16)₁) with a polynomial expression:

$$\sigma = a_0 + c_1 x_1^2 + c_1 x_2^2 + c_2 x_1^4 + c_2 x_2^4 + c_3 x_1^6 + c_3 x_2^6, \quad (21)$$

from which F^* can be obtained by integrating (13).

4.7. Energy in discrete form. From (14) we obtain a linear problem for F in the form (1) as described below. Considering the discretization on the mesh, equation (14) can be transformed into

$$E(F) = \frac{1}{2} \sum_{n=1}^N a_{\alpha\beta}(n) F_{,\alpha}(n) F_{,\beta}(n) + \sum_{n=1}^N p(n) F(n). \quad (22)$$

4.8. Stationarity in discrete form. Considering condition (15), we obtain

$$\sum_{n=1}^N a_{\alpha\beta}(n) F_{,\beta}(n) + p(n) = 0. \quad (23)$$

A system of the form (1) can be obtained from (23) considering that the matrix A is the coefficient matrix of F for the internal part of the mesh, that is the part where the values of F are unknown, and the vector b is the coefficient vector of $F^* = F/\partial\Omega$ to which the load p is subtracted.

For the evaluation of the term $\sum_{n=1}^N a_{\alpha\beta}(n) F_{,\beta}(n)$ in (23), we considered for each node:

$$a_{\alpha\beta} F_{,\alpha} F_{,\beta} = \frac{\hat{f}^0_{,22} \sum_m F_{,1} F_{,1} + \hat{f}^0_{,11} \sum_m F_{,2} F_{,2} + 2\hat{f}^0_{,12} \sum_m F_{,1} F_{,2}}{\text{area}(\Omega_j)}, \quad j \in \{1, 2, \dots, n\}, \quad (24)$$

where $\hat{f}^0_{,ij}$ is the Hessian matrix at the node, and $F_{,\alpha}$, $F_{,\beta}$ are the covariant component of the gradient of F evaluated in the triangular element of the mesh that are partially included in the dual element of the node (Figure 5).

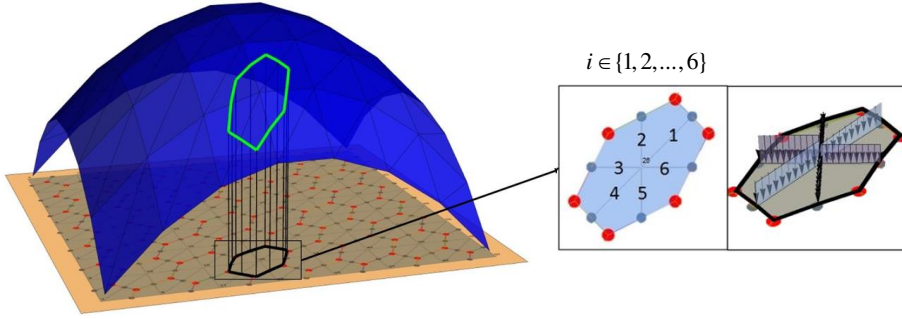


Figure 5. Curvature approximation.

4.9. Stress optimization. To find the best equilibrium solution, the boundary values will be selected by an optimization procedure. The optimization function density we select, encouraging the concavity of the stress function, is (see [Figure 6](#))

$$\Psi(x_1, x_2) = \begin{cases} 0 & x_1 \leq 0, x_2 \leq 0 \\ x_1^2 & x_1 > 0, x_2 < 0 \\ x_2^2 & x_1 < 0, x_2 > 0 \\ x_1^2 + x_2^2 & x_1 > 0, x_2 > 0, \end{cases} \quad (25)$$

with

$$x_1 = \frac{H_{11} + H_{22}}{2} + \sqrt{\left(\frac{H_{11} + H_{22}}{2}\right)^2 + H_{12}^2}, \quad x_2 = \frac{H_{11} + H_{22}}{2} - \sqrt{\left(\frac{H_{11} + H_{22}}{2}\right)^2 + H_{12}^2}, \quad (26)$$

where H_{ij} are the components of the Hessian of the stress function F .

The objective function to minimize is

$$\Phi_F = \int_{\Omega} \Psi(x_1, x_2) d\Omega. \quad (27)$$

The smaller the value found during the optimization process, the more the Hessian matrix will be closer to being a negative semidefinite matrix. In [Figure 6](#) the objective function is depicted.

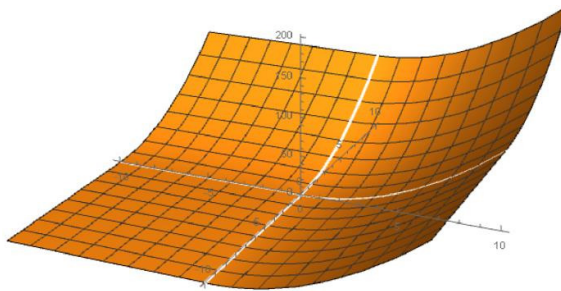


Figure 6. Density $\Psi(x_1, x_2)$ of the objective function Φ_F .

By means of equation (2) we can evaluate the stress function F . Having adopted two different meshes, two stress functions are obtained. Therefore, F will be evaluated by superimposing these two functions. If the deducted stress function is concave, then the vault is purely compressed and the current solution is accepted. Otherwise, we start a new iteration process considering the form function as the unknown. With a similar procedure as described above by changing the role of the form and of the stress function, a new form is obtained. In this case, the objective function to be optimized is

$$\Phi_f = \int_{\Omega} (f - f^0)^2 d\Omega, \quad (28)$$

that is, the mean squared deviation from the middle surface.

5. Examples

To illustrate the method, we consider two simple examples: a cloister vault and a cross vault.

5.1. Cloister vault. The optimization procedure exposed in Section 4 is adapted for the cloister vault starting with an initial form, that is, the middle surface of the vault structure in Figure 7 (see [Angelillo et al. 2013]):

$$f^0 = \begin{cases} \frac{L}{R} \sqrt{R^2 - x_1^2}, & |x_1| \geq |x_2|, \\ \frac{L}{R} \sqrt{R^2 - x_2^2}, & |x_1| < |x_2|, \end{cases} \quad (29)$$

taking the geometrical parameters $L = 5$ and $R = 5.5$ as the dimensions of the square planform and the apical rise of the cloister vault.

Two primal meshes of the form (see Figure 3) are introduced on the planform with $e = 0.5$. The domain of the vault and the meshes are extended with a strip of elements of width 0.5 on all sides. The applied transverse load is uniform with $p = -1$. By using the objective function (25), the optimization process at the first iteration gives $\Phi_F = 236$. By means of equation (2) we obtain the stress functions associated to the two primal meshes (Figure 8).

Superimposing linearly the two stress functions, we have the resulting stress function (Figure 9, left). By taking the convex hull, we transform this surface into a concave function (Figure 9, right).

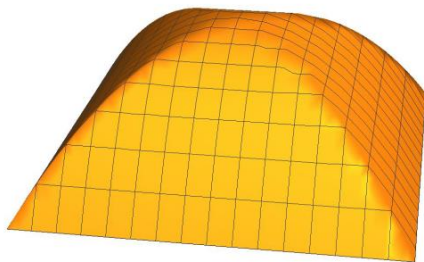


Figure 7. Starting form function f^0 .



Figure 8. Stress functions due to mesh 1 and mesh 2.

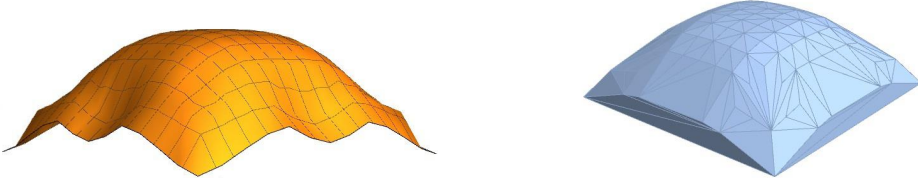


Figure 9. Optimized stress function F^0 related to f^0 (left) and its convex hull result (right).

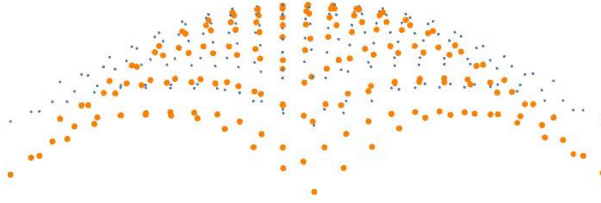


Figure 10. Initial convexified stress function (light blue points), and final stress function considering the uniform load superposition (orange points).

To avoid flat areas, where the curvature vanishes (giving possible numerical problems in the subsequent evaluations) we increase the stress function by a uniform pressure tuned by coefficient β :

$$F_{\text{new}} = F - \left[\frac{1}{2} \beta F_{\text{med}} (x_1^2 + x_2^2) \right]. \quad (30)$$

In particular, we take $\beta = 0.1$.

In [Figure 10](#), the stress function obtained after the convex hull and the uniform load superposition, is compared with the one corresponding to the convex hull procedure. In [Figure 11](#) (left) the final stress function is depicted.

In the second step, this stress function F is considered as assigned and the form function f as the unknown. In this phase, the optimization function (28) is considered. As a result of the optimization we have, in this case, $\Phi_f = 18$. The results for the optimized form function are displayed in [Figure 11](#) (right). In [Figure 12](#) (left) such surface is compared with the starting shape f .

To improve the result, a new optimization cycle is performed. The new optimization cycle on the stress functional (27) gives $\Phi_F = 186$ and after the convex hull, the final stress function of [Figure 12](#) (right) that we use for the evaluation of the form function is obtained.

Therefore, a new iteration adopting the optimization functional (28), whose unknown is the form function, is executed. Performing the optimization, we get $\Phi_f = 2$. As a result, [Figure 13](#) (left) shows

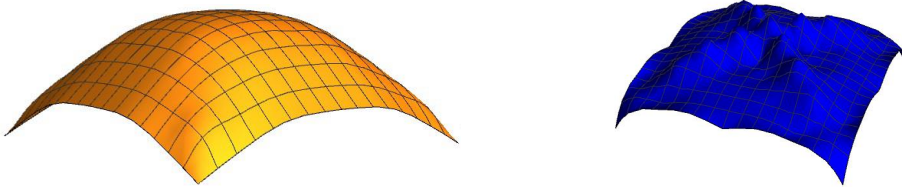


Figure 11. Left: final stress function at step 1. Right: optimized form function.

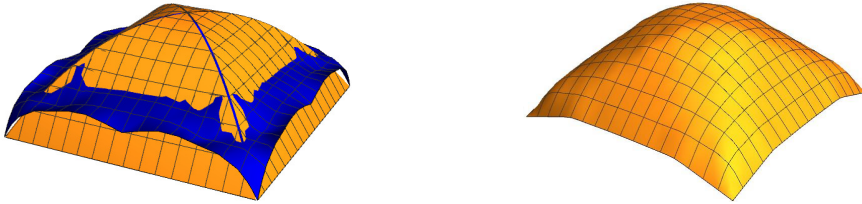


Figure 12. Left: comparison between the new form function (blue) and the starting form f^0 . Right: final stress function after at step 2.

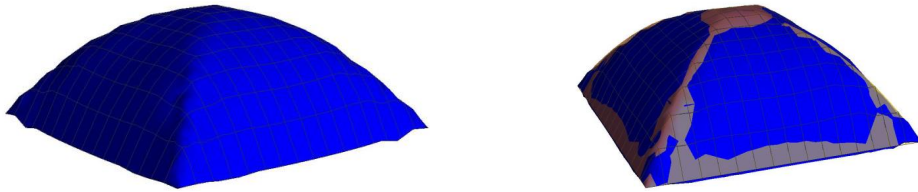


Figure 13. Left: final form function. Right: comparison between the final form function (blue) and the starting form f^0 .

the final optimized form, while in [Figure 13](#) (right) this surface is compared with the starting surface. We can observe that the form function is very close to the surface of the vault and that a tolerance value of less than 0.1 is verified at each point. Finally, [Figure 14](#) shows the envelope field of the principal direction of stress corresponding to the final stress function represented in [Figure 12](#) (right).

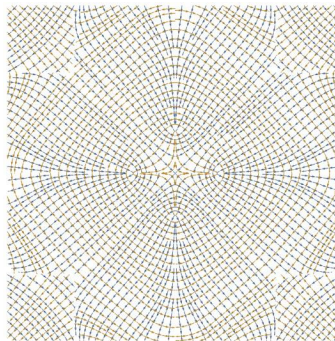


Figure 14. Principal stress lines.

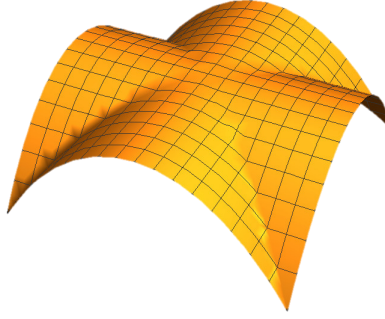


Figure 15. Starting form function f^0 for the cloister vault.

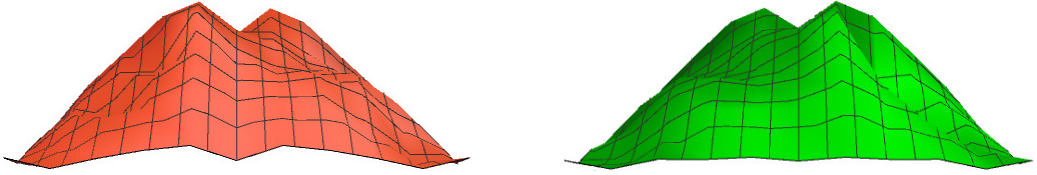


Figure 16. Stress functions due to mesh 1 and mesh 2.

5.2. Cross vault. As in the previous case, for the cross vault we choose the middle surface of the same vault as the initial shape from which starting the optimization process as in Figure 15, as exposed in [Angelillo et al. 2013]:

$$f^0 = \begin{cases} \frac{L}{R} \sqrt{R^2 - x_1^2}, & |x_1| < |x_2|, \\ \frac{L}{R} \sqrt{R^2 - x_2^2}, & |x_1| \geq |x_2|. \end{cases} \quad (31)$$

for the side and the radius of the vault we put $L = 5$ and $R = 7$.

The procedure for this example is similar to the previous one, therefore the main features and results will be summarized briefly in the following. We have two primal meshes with element size $e = 0.5$ and a transverse load $p = -1$. The optimization at the first step gives $\Phi_F = 291$. By using (2), the two stress functions corresponding to the two primal meshes are depicted in Figure 16. Superimposing them we obtain the stress function of Figure 17 (left). In Figure 17 (right) the stress function obtained through the convex hull procedure is shown.

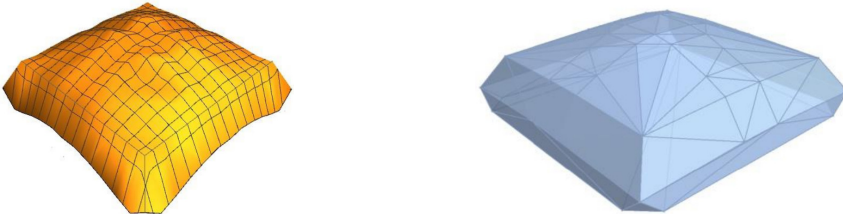


Figure 17. Left: optimized stress function F^0 associate to f^0 . Right: convex hull result of the stress function.

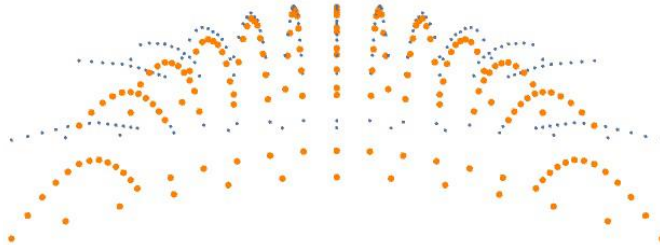


Figure 18. Initial convexified stress function (points in light blue), and final stress function considering the uniform load superposition (points in orange).

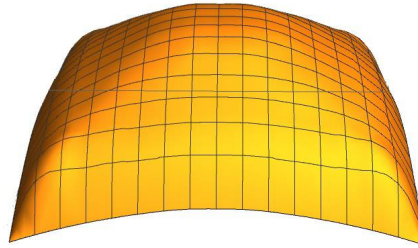


Figure 19. Final stress function at step 1.

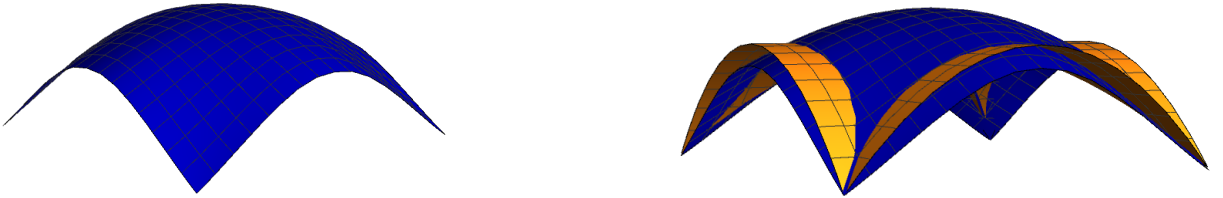


Figure 20. Left: optimized form function. Right: comparison between the new form function (in blue) and the initial one.

The flat areas are eliminated adding to the stress function a uniform pressure (see (30)) and taking $\beta = 0.1$. In Figure 18 the stress function obtained with the superposition is compared with the one derived through the convex hull. In Figure 19 the final stress function is depicted.

In the second step, the optimization of the function (28) gives $\Phi_f = 8$. The results obtained for the optimized form function are reported in Figure 20 (left); in Figure 20 (right), such form is compared with the starting shape f^0 .

The new optimization of the objective function (27) with respect to the stress function gives $\Phi_F = 256$, to which corresponds the stress function depicted in Figure 21.

The new optimization of the form function with respect to the objective function (28) gives $\Phi_f = 1$. The final optimized form is displayed in Figure 22 (left); the two forms are compared in Figure 22 (right). The isostatic stress lines corresponding to the final stress function are reported in Figure 23.

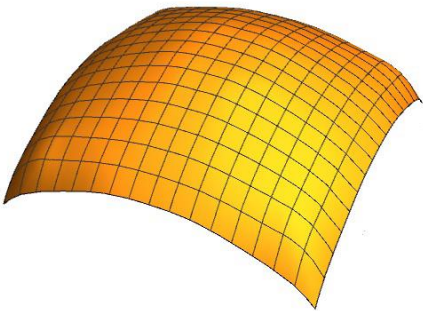


Figure 21. Final stress function at step 2 after concavification.

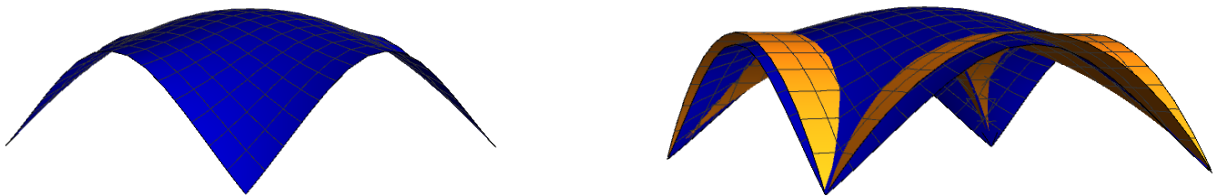


Figure 22. Left: final form function (left). Right: comparison between the final form function (blue) and the starting form f^0 .

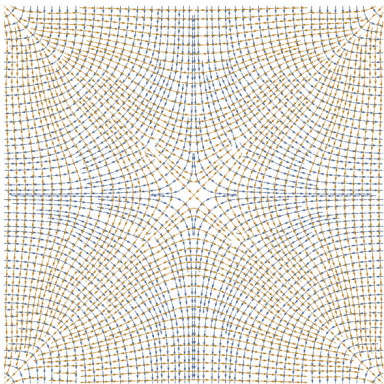


Figure 23. Principal stress lines.

6. Conclusions

The present work develops an automated numerical method for the analysis of thin masonry shells. The model of material adopted for masonry is the NRNT, for which the limit analysis theorems are still valid. Accordingly, the study focuses on the application of the static theorem to masonry vaults.

In detail, the proposed method is devoted to the automatic generation of a class of purely compressive stress regimes, which are balanced with the load. As a consequence, the structure is safe and members of this statically admissible stresses may be used to assess the geometric degree of safety of the structure and to estimate bounds on the thrust forces exerted by the structure on its boundary.

By taking up the simplified model of Heyman, the equilibrium problem for the membrane has been formulated in terms of projected stresses defined on the planform of the vault. The search for the stresses reduces to the solution of a second-order pde, in terms of the stress potential F . In order that the membrane stress on S be compressive, the potential F must be concave. As for the thrust line in an arch, the surface S is not fixed and may be changed, given that it remains inside the masonry.

Under these assumptions, the whole class of equilibrated stress regimes for a masonry shell, is obtained by moving and deforming S inside the masonry, and also, for any fixed shape, by changing the boundary data for F , that is the distribution of thrust forces along the boundary. The unilateral NT condition require that F lies in between the extrados and intrados surfaces of the vault and that be moreover concave. Such last constraint is, in general, not satisfied on a given shape for given loads. In such a case, the shape has been modified to fit the constraint.

The search for a feasible stress state on a convenient membrane surface, has been conducted so far iteratively, by trial and error; this sort of manual procedure, based on a skillful ansatz either on the initial shape (that is, on f) or on the initial projected stress (that is, on F), requires a substantial effort and may be unrewarded.

Thus, the development of a computer code capable of handling numerically the interplay of the shape f and the stress potential F , has been the main object of the present work.

In particular, in the present work, the cases of cloister and cross vaults are considered as examples of application of the method. For such a special case, easy and efficient methods to evaluate the equilibrium do not exist, and the simplified slicing technique gives rather inaccurate estimates of the geometrical factor of safety. The proposed method, in these simple cases, appears to be rather efficient.

References

- [Angelillo 2014] M. Angelillo, “Practical applications of unilateral models to Masonry equilibrium”, pp. 109–210 in *Mechanics of masonry structures*, vol. 551, edited by M. Angelillo, Springer, Vienna, 2014.
- [Angelillo 2015] M. Angelillo, “Static analysis of a Guastavino helical stair as a layered masonry shell”, *Compos. Struct.* **119** (2015), 298–304.
- [Angelillo 2016] M. Angelillo, “The equilibrium of helical stairs made of monolithic steps”, *Int. J. Archit. Herit.* **10**:6 (2016), 675–687.
- [Angelillo and Fortunato 2004] M. Angelillo and A. Fortunato, “Equilibrium of masonry vaults”, pp. 105–111 in *Novel approaches in civil engineering: lecture notes in applied and computational mechanics*, vol. 14, edited by M. Frémond and F. Maceri, Springer, Berlin, Heidelberg, 2004.
- [Angelillo et al. 2010] M. Angelillo, L. Cardamone, and A. Fortunato, “A numerical model for masonry-like structures”, *J. Mech. Mater. Struct.* **5**:4 (2010), 583–615.
- [Angelillo et al. 2013] M. Angelillo, E. Babilio, and A. Fortunato, “Singular stress fields for masonry-like vaults”, *Contin. Mech. Therm.* **25**:2-4 (2013), 423–441.
- [Angelillo et al. 2014] M. Angelillo, A. Fortunato, A. Montanino, and M. Lippiello, “Singular stress fields in masonry structures: Derand was right”, *Meccanica (Milano)* **49**:5 (2014), 1243–1262.
- [Angelillo et al. 2016] M. Angelillo, E. Babilio, A. Fortunato, M. Lippiello, and A. Montanino, “Analytic solutions for the stress field in static sandpiles”, *Mech. Mater.* **95** (2016), 192–203.
- [Block 2009] P. Block, *Thrust network analysis: exploring three-dimensional equilibrium*, PhD dissertation, Dept. of Architecture, Massachusetts Institute of Technology, Cambridge, USA, 2009, Available at <https://dspace.mit.edu/handle/1721.1/49539>.

- [Block and Lachauer 2014] P. Block and L. Lachauer, “Three-dimensional funicular analysis of masonry vaults”, *Mech. Res. Commun.* **56** (2014), 53–60.
- [Block et al. 2006] P. Block, T. Ciblac, and J. Ochsendorf, “Real-time limit analysis of vaulted masonry buildings”, *Comput. Struct.* **84**:29-30 (2006), 1841–1852.
- [Brandonisio et al. 2015] G. Brandonisio, E. Mele, and A. De Luca, “Closed form solution for predicting the horizontal capacity of masonry portal frames through limit analysis and comparison with experimental test results”, *Eng. Fail. Anal.* **55** (2015), 246–270.
- [Bruggi and Taliercio 2015] M. Bruggi and A. Taliercio, “Analysis of no-tension structures under monotonic loading through an energy-based method”, *Comput. Struct.* **159** (2015), 14–25.
- [Calladine 2005] C. R. Calladine, “Preliminary structural analysis of a Guastavino spiral staircase shell”, in *Essays in the history of the theory of structures, in honour of Jacques Heyman*, Instituto Juan de Herrera, Madrid, 2005.
- [Cennamo et al. 2017] C. Cennamo, M. Angelillo, and C. Cusano, “Structural failures due to anthropogenic sinkholes in the urban area of Naples and the effect of a FRP retrofitting”, *Compos. B Eng.* **108** (2017), 190–199.
- [Como 1992] M. Como, “Equilibrium and collapse analysis of masonry bodies”, *Meccanica (Milano)* **27**:3 (1992), 185–194.
- [De Goes et al. 2013] F. De Goes, P. Alliez, H. Owahdi, and M. Desbrun, “On the equilibrium of simplicial masonry structures”, *ACM Trans. Graph.* **32**:4 (2013), article 93.
- [De Serio et al. 2018] F. De Serio, M. Angelillo, A. Gesualdo, A. Iannuzzo, G. Zuccaro, and M. Pasquino, “Masonry structures made of monolithic blocks with an application to spiral stairs”, *Meccanica (Milano)* **53**:8 (2018), 2171–2191.
- [DeJong and Dimitrakopoulos 2014] M. J. DeJong and E. G. Dimitrakopoulos, “Dynamically equivalent rocking structures”, *Earthq. Eng. Struct. Dyn.* **43**:10 (2014), 1543–1563.
- [Fortunato et al. 2014] A. Fortunato, F. Fraternali, and M. Angelillo, “Structural capacity of masonry walls under horizontal loads”, *Ing. Sismica* **31**:1 (2014), 41–49.
- [Fortunato et al. 2016] A. Fortunato, E. Babilio, M. Lippiello, A. Gesualdo, and M. Angelillo, “Limit analysis for unilateral masonry-like structures”, *Open Construct. Build. Technol. J.* **10**:Suppl 2: M12 (2016), 346–362.
- [Fortunato et al. 2018] A. Fortunato, F. Fabbrocino, M. Angelillo, and F. Fraternali, “Limit analysis of masonry structures with free discontinuities”, *Meccanica (Milano)* **53**:7 (2018), 1793–1802.
- [Fraternali 2010] F. Fraternali, “A thrust network approach to the equilibrium problem of unreinforced masonry vaults via polyhedral stress functions”, *Mech. Res. Commun.* **37**:2 (2010), 198–204.
- [Fraternali et al. 2002a] F. Fraternali, M. Angelillo, and A. Fortunato, “A lumped stress method for plane elastic problems and the discrete-continuum approximation”, *Int. J. Solids Struct.* **39**:25 (2002), 6211–6240.
- [Fraternali et al. 2002b] F. Fraternali, M. Angelillo, and G. Rocchetta, “On the stress skeleton of masonry vaults and domes”, in *Proceedings of the Seventh Pan American Congress of Applied Mechanics (PACAM VII)* (Temuco, Chile), 2002.
- [Gesualdo et al. 2014] A. Gesualdo, A. Iannuzzo, M. Monaco, and M. T. Savino, “Dynamic analysis of freestanding rigid blocks”, in *The Twelfth International Conference on Computational Structures Technology* (Naples, Italy), vol. 106, 2014.
- [Gesualdo et al. 2017] A. Gesualdo, C. Cennamo, A. Fortunato, G. Frunzio, M. Monaco, and M. Angelillo, “Equilibrium formulation of masonry helical stairs”, *Meccanica (Milano)* **52**:8 (2017), 1963–1974.
- [Gesualdo et al. 2018a] A. Gesualdo, A. Iannuzzo, V. Minutolo, and M. Monaco, “Rocking of freestanding objects: theoretical and experimental comparisons”, *J. Theor. Appl. Mech. (Warsaw)* **56**:4 (2018), 977–991.
- [Gesualdo et al. 2018b] A. Gesualdo, A. Iannuzzo, M. Monaco, and F. Penta, “Rocking of a rigid block freestanding on a flat pedestal”, *J. Zhejiang Univ. Sci. A* **19**:5 (2018), 331–345.
- [Giaquinta and Giusti 1985] M. Giaquinta and E. Giusti, “Researches on the equilibrium of masonry structures”, *Arch. Ration. Mech. Anal.* **88**:4 (1985), 359–392.
- [Heyman 1966] J. Heyman, “The stone skeleton”, *Int. J. Solids Struct.* **2**:2 (1966), 249–279.
- [Heyman 2012] J. Heyman, “The membrane analysis of thin masonry shells”, *Nuts Bolts Construct. Hist.* **1** (2012), 281–283.
- [Iannuzzo et al. 2018] A. Iannuzzo, M. Angelillo, E. De Chiara, F. De Guglielmo, F. De Serio, F. Ribera, and A. Gesualdo, “Modelling the cracks produced by settlements in masonry structures”, *Meccanica (Milano)* **53**:7 (2018), 1857–1873.

- [Kooharian 1952] A. Kooharian, “Limit analysis of voussoir (segmental) and concrete arches”, *J. Am. Concr. Inst.* **24**:4 (1952), 317–328.
- [Livesley 1978] R. K. Livesley, “Limit analysis of structures formed from rigid blocks”, *Int. J. Numer. Methods Eng.* **12**:12 (1978), 1853–1871.
- [Marmo and Rosati 2017] F. Marmo and L. Rosati, “Reformulation and extension of the thrust network analysis”, *Comput. Struct.* **182** (2017), 104–118.
- [Marmo et al. 2018] F. Marmo, D. Masi, and L. Rosati, “Thrust network analysis of masonry helical staircases”, *Int. J. Archit. Herit.* **12**:5 (2018), 828–848.
- [Miki et al. 2015] M. Miki, T. Igarashi, and P. Block, “Parametric self-supporting surfaces via direct computation of airy stress functions”, *ACM Trans. Graph.* **34**:4 (2015), article 89.
- [Monaco et al. 2014] M. Monaco, M. Guadagnuolo, and A. Gesualdo, “The role of friction in the seismic risk mitigation of freestanding art objects”, *Nat. Hazards* **73**:2 (2014), 389–402.
- [O’Dwyer 1999] D. W. O’Dwyer, “Funicular analysis of masonry vaults”, *Comput. Struct.* **73**:1-5 (1999), 187–197.
- [Pucher 1934] A. Pucher, “Über der spannungszustand in gekrümmten flächen”, *Beton u Eisen* **33** (1934), 298–304.
- [Vouga et al. 2012] E. Vouga, M. Höbinger, J. Wallner, and H. Pottmann, “Design of self-supporting surfaces”, *ACM Trans. Graph.* **31**:4 (2012), article 87.

Received 24 Mar 2019. Revised 3 Oct 2019. Accepted 18 Oct 2019.

ELENA DE CHIARA: elenadechiara@gmail.com

Department of Civil Engineering, University of Salerno, Via Giovanni Paolo II, 132, 84084 Fisciano, Italy

CLAUDIA CENNAO: claudia.cennamo@unicampania.it

Department of Architecture and Industrial Design, University of Campania “Luigi Vanvitelli”, 81031 Aversa, Italy

ANTONIO GESUALDO: gesualdo@unina.it

Department of Structures for Engineering and Architecture, University of Naples Federico II, Via Claudio 21 (buildings 6-7), 80125 Naples, Italy

ANDREA MONTANINO: andrea.montanino@polimi.it

Department of Structures for Engineering and Architecture, University of Naples Federico II, Via Claudio 21 (buildings 6-7), 80125 Naples, Italy

CARLO OLIVIERI: colivieri@unisa.it

Department of Civil Engineering, University of Salerno, Via Giovanni Paolo II, 132, 84084 Fisciano, Italy

ANTONIO FORTUNATO: a.fortunato@unisa.it

Dipartimento di Ingegneria Civile, University of Salerno, Via Giovanni Paolo II, 132, 84084 Fisciano, Italy

JOURNAL OF MECHANICS OF MATERIALS AND STRUCTURES

msp.org/jomms

Founded by Charles R. Steele and Marie-Louise Steele

EDITORIAL BOARD

ADAIR R. AGUIAR	University of São Paulo at São Carlos, Brazil
KATIA BERTOLDI	Harvard University, USA
DAVIDE BIGONI	University of Trento, Italy
MAENGHYO CHO	Seoul National University, Korea
HUILING DUAN	Beijing University
YIBIN FU	Keele University, UK
IWONA JASIUK	University of Illinois at Urbana-Champaign, USA
DENNIS KOCHMANN	ETH Zurich
MITSUTOSHI KURODA	Yamagata University, Japan
CHEE W. LIM	City University of Hong Kong
ZISHUN LIU	Xi'an Jiaotong University, China
THOMAS J. PENCE	Michigan State University, USA
GIANNI ROYER-CARFAGNI	Università degli studi di Parma, Italy
DAVID STEIGMANN	University of California at Berkeley, USA
PAUL STEINMANN	Friedrich-Alexander-Universität Erlangen-Nürnberg, Germany
KENJIRO TERADA	Tohoku University, Japan

ADVISORY BOARD

J. P. CARTER	University of Sydney, Australia
D. H. HODGES	Georgia Institute of Technology, USA
J. HUTCHINSON	Harvard University, USA
D. PAMPLONA	Universidade Católica do Rio de Janeiro, Brazil
M. B. RUBIN	Technion, Haifa, Israel

PRODUCTION production@msp.org

SILVIO LEVY Scientific Editor


Cover photo: Mando Gomez, www.mandolux.com

See msp.org/jomms for submission guidelines.

JoMMS (ISSN 1559-3959) at Mathematical Sciences Publishers, 798 Evans Hall #6840, c/o University of California, Berkeley, CA 94720-3840, is published in 10 issues a year. The subscription price for 2019 is US \$635/year for the electronic version, and \$795/year (+\$60, if shipping outside the US) for print and electronic. Subscriptions, requests for back issues, and changes of address should be sent to MSP.

JoMMS peer-review and production is managed by EditFlow® from Mathematical Sciences Publishers.

PUBLISHED BY

 **mathematical sciences publishers**
nonprofit scientific publishing

<http://msp.org/>

© 2019 Mathematical Sciences Publishers

Preface	MAURIZIO ANGELILLO and SANTIAGO HUERTA FERNÁNDEZ	601
Studying the dome of Pisa cathedral via a modern reinterpretation of Durand-Claye's method	DANILO AITA, RICCARDO BARSOTTI and STEFANO BENNATI	603
Experimental and numerical study of the dynamic behaviour of masonry circular arches with non-negligible tensile capacity	ALEJANDRA ALBUERNE, ATHANASIOS PAPPAS, MARTIN WILLIAMS and DINA D'AYALA	621
Influence of geometry on seismic capacity of circular buttressed arches	GIUSEPPE BRANDONISIO and ANTONELLO DE LUCA	645
Failure pattern prediction in masonry	GIANMARCO DE FELICE and MARIALAURA MALENA	663
Energy based fracture identification in masonry structures: the case study of the church of "Pietà dei Turchini"	ANTONINO IANNUZZO	683
Displacement capacity of masonry structures under horizontal actions via PRD method	ANTONINO IANNUZZO, CARLO OLIVIERI and ANTONIO FORTUNATO	703
Automatic generation of statically admissible stress fields in masonry vaults	ELENA DE CHIARA, CLAUDIA CENNAMO, ANTONIO GESUALDO, ANDREA MONTANINO, CARLO OLIVIERI and ANTONIO FORTUNATO	719
Limit analysis of cloister vaults: the case study of Palazzo Caracciolo di Avellino	ANTONIO GESUALDO, GIUSEPPE BRANDONISIO, ANTONELLO DE LUCA, ANTONINO IANNUZZO, ANDREA MONTANINO and CARLO OLIVIERI	739
The rocking: a resource for the side strength of masonry structures	MARIO COMO	751